



# A Comparative Study of Pulse and DC Electroplating of Zn onto Mild Steel for Improved Corrosion Resistance

Pundrikaksha Upadhyay<sup>1</sup> · Anushri Nag<sup>2</sup> ·  
Atanu Banerjee<sup>2</sup> · Anindya Basu<sup>3</sup> · Sanjeev Das<sup>4</sup> ·  
Archana Mallik<sup>1</sup>

Received: 30 April 2023 / Accepted: 4 September 2023 / Published online: 25 September 2023  
© The Indian Institute of Metals - IIM 2023

**Abstract** In the current study, Zn electrodeposition was done from an acidic sulfate bath onto mild steel at a pH of 3.5. The Zn coating was done in both direct current (DC) and the pulsed current mode to investigate whether the two techniques would lead to a difference in the corrosion behavior of the plated films. The range of deposition current density was obtained through a systematic cyclic voltammetry (CV). The chosen current density values were  $-50$ ,  $-150$ ,  $-180$ , and  $-250$  mA/cm<sup>2</sup>. Pulse deposition was done after the DC deposition at the average current density of  $-180$  mA/cm<sup>2</sup> at different duty cycles, frequencies and peak current densities. The thickness of the coating was measured by using a surface profilometer and was found to be in the range of 10–28  $\mu$ m. Phase, structure and composition of the deposition were characterized by XRD, SEM and elemental mapping. Tafel polarization technique and electrochemical impedance spectroscopy were done to study the corrosion rate and mechanism in 3.5 wt% NaCl. A marginal increase in corrosion resistance was observed for pulse-deposited films as compared

to DC-deposited ones. Films deposited at  $-180$  mA/cm<sup>2</sup> and a combination of duty cycle, i.e., peak current density of  $-720$  mA/cm<sup>2</sup> and at the frequency of 75 Hz, were found to have the optimum anti-corrosion performance.

**Keywords** Electroplating · Corrosion · Galvanization

## 1 Introduction

Galvanizing is one of the techniques which prevents mild steel from corrosion, where a layer of zinc is coated onto it. The zinc coating can be obtained either by hot dip galvanizing (HDG), metalizing (zinc spraying), mechanical plating or electrogalvanizing to provide sacrificial protection [1]. HDG is the immersion of steel in a molten bath of zinc or zinc alloy bath at 450 °C to achieve the coat through batch or continuous processing [2]. During HDG, a combination of alloy and intermetallics of Fe–Zn layers gets developed in the interface of steel and Zn coating. This interface layer is generally hard; hence, the usual abrasive does not damage the deposited surface even if it can be harmful to the soft pure Zn on the top [3]. The coating thickness lies in the range of 80–100  $\mu$ m depending on the duration of dipping [4]. The variations in coating thickness give an adverse effect on weldability and formability. Due to the above disadvantages of HDG, electrogalvanizing (EG) is gaining more attention. The coatings obtained through EG are generally uniform (usually in range of 10–20  $\mu$ m) and shiny, but the life may be less, i.e., several months to some years compared to HDG. However, HDG is more expensive and corrosion resistive due to the high thickness of the Zn layer than EG. Hence, the research in EG has not been optimized yet.

✉ Pundrikaksha Upadhyay

Archana Mallik  
archananitrkl@gmail.com

- <sup>1</sup> Electrometallurgy and Corrosion Laboratory, Department of Metallurgical and Materials Engineering, National Institute of Technology Rourkela, Rourkela 769008, India
- <sup>2</sup> R&D, Tata Steel Ltd., Jamshedpur 831001, India
- <sup>3</sup> Department of Metallurgical and Materials Engineering, National Institute of Technology Rourkela, Rourkela 769008, India
- <sup>4</sup> AMC Laboratory, Department of Metallurgical and Materials Engineering, National Institute of Technology Raipur, Chhattisgarh 492010, India

In the EG process, zinc gets electroplated onto mild steel by either passing a direct current (DC) or potential through a zinc solution. The parameters which generally affect the deposit characteristics are current density (CD), bath temperature, distance between the electrodes, electrolyte type, pH of the bath and additives, etc. A few studies on the effect of these parameters are reviewed briefly and presented in the following section. The effect of deposition potential on nucleation and formation of Zn reported that 2D and 3D nucleation was followed when potential increased from 0.3 V to 0.55 V and above, respectively [5]. It was found that formation of long dendrites and size dispersion occurred with increase in CD, whereas an increase in temperature provided a decrease in average dendritic length [6]. Another interesting study on the use of waste zinc to EG has been reported which has been found to be effective in terms of coating characteristics. The approach failed as the production of pure zinc from waste source is difficult and expensive [7]. In the above studies, the main focus was on the effect of deposition parameters on zinc film characteristics and rare reporting on the corrosion behavior was made. Most of the research findings for improved corrosion resistance are either through alloying or composite film fabrication. Alloying the film with Ni decreased the corrosion current from a value of 144 to 59  $\mu\text{A}/\text{cm}^2$  and corrosion potential from  $-1$  to  $-0.8$  V with increase of Ni content from 9 to 15.9 wt% when tested in 3.5 wt% NaCl solution [8]. Jyothender et al. reported that the addition of carbon nanotubes (CNT) improved corrosion resistance of the coatings by forming Zn-CNT composite coatings [9]. A similar study was done to incorporate graphene oxide (GO) in place of CNT, and it was found that addition of GO showed an increase in polarization resistance and a drop-in corrosion rate [10]. In another recent study, incorporation of nano- $\text{Al}_2\text{O}_3$  powder as a reinforcement was done and it was found that corrosion rate decreased from 0.0008 mm/yr to 0.0003 mm/yr [11]. Hence, alloying and reinforcement addition could be alternative approaches for increasing the corrosion resistance of EG steel. However, if by any means the alloying/composite can be avoided (which may lead to faster de-zincification), then this would add to the economy of the process. Hence, exploration of process parameter variations could be an alternative approach.

For commercial practices, current density is the main operating parameter with different bath compositions. If this parameter can be explored extensively to improve the corrosion resistance, then a lot of cost saving can be done and one such way is pulse electroplating (PEP). In pulse electroplating, the swift alternating of the electrical current/CD between two different values would result in a series of pulses of equal amplitude, duration and polarity, separated by zero current. N. fathy et al. explored the technique to deposit ZnS thin films and observed grain refinement in the films as compared to DC electrodeposition [12]. Attempt

has also been made to coat Zn–Ni– $\text{Al}_2\text{O}_3$  nano-composite films at a peak current density of 16.6–17.1  $\text{A}/\text{m}^2$  and pulse frequency of 105–120 Hz in the presence of ultrasound (35–50 W) where only reporting of alumina incorporation was the main focus [13].

From this limited findings, it can be assessed that the technique of pulse plating has not been explored extensively for EG. Hence, in the current study PEP has been adopted to deposit zinc and check the effect of its parameters on the evolution of properties of the as-deposited coatings. At first zinc deposition was done by DC at different CDs and an optimum value was chosen to do the PEP. Based on the evaluated optimum CD, the parameters of PEP, i.e., peak CD, duty cycle and frequency, were chosen. Finally, it was assessed whether the technique could improve the corrosion resistance of films.

## 2 Materials and Methodology

Mild steel (MS) plate with an exposed area of 0.79  $\text{cm}^2$  was used as the substrate. EG of pure Zn coating was performed in a three-electrode cell with a zinc counter electrode and saturated calomel electrode as the reference electrode. The analysis was carried out in a bath containing  $\text{ZnSO}_4 \cdot 7\text{H}_2\text{O}$  (250 g/l),  $\text{ZnCl}_2$  (6 g/l),  $\text{H}_3\text{BO}_3$  (30 g/l) and SDS (0.5 g/l) as the additive. The chosen composition was analyzed through a thermodynamic study by using Factsage software and is presented in Fig. 1. From the diagram, it was analyzed that without additives, ZnO precipitation would be possible. However, in the presence of additives, significant phases were mostly aqueous, which could be the advantage of adding these reagents. Further, the zinc ion concentration is not affected by the addition of boric acid or SDS, nor are they making any complexes. Hence, the addition of the reagents would lead to a bright and uniform deposit which has been observed in later sections. DC deposition was done at different deposition current densities ( $-50$ ,  $-150$ ,  $-180$  and  $-250$   $\text{mA}/\text{cm}^2$ ) which were obtained from cyclic voltammetry (CV), whereas pulse deposition was done with different parameters as mentioned in Table 1. The table also includes the sample nomenclature.

Scanning electron microscope (SEM) images of the coated surface were obtained by a JEOL JSM-6480 LV. The weight percentage of elements and elemental mapping were carried out by energy-dispersive spectroscopy (EDS) fitted with the SEM. X-ray diffraction (XRD) profiles were obtained by Bruker AXS D8 Advance Davinci Design diffractometer fitted with Co- $\text{K}\alpha$  target in the range of 10–100° at a scan rate of 10°/min with a step size of 0.02°. The thickness and surface roughness of the coated film were acquired by the Veeco dektak 150 surface stylus profiler. To analyze the adherence of the coatings onto the substrate, the scratch

**Fig. 1** Electrochemical phase diagrams of Zn–H<sub>2</sub>O **a** without and **b** with additives

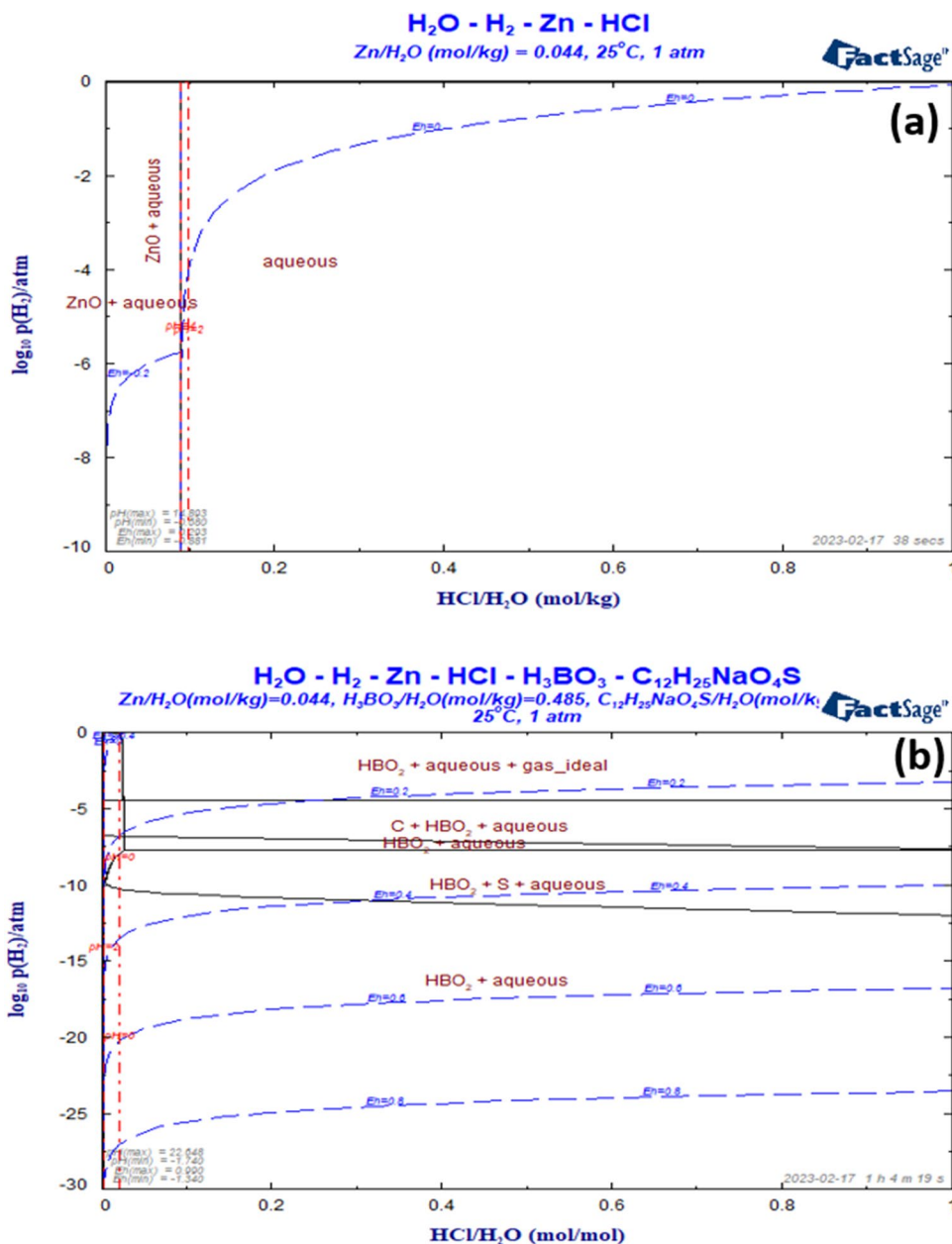


**Table 1** Nomenclature for pulse coating based on the operating parameter

| Duty cycle | F (Hz)                               |                                      |                                      |
|------------|--------------------------------------|--------------------------------------|--------------------------------------|
|            | 25                                   | 75                                   | 200                                  |
| 25%        | $t_{on} = 10 \text{ ms}$             | $t_{on} = 3.33 \text{ ms}$           | $t_{on} = 1.25 \text{ ms}$           |
|            | $t_{off} = 30 \text{ ms}$            | $t_{off} = 10 \text{ ms}$            | $t_{off} = 3.75 \text{ ms}$          |
|            | PCD = -720 mA/cm <sup>2</sup><br>17A | PCD = -720 mA/cm <sup>2</sup><br>17B | PCD = -720 mA/cm <sup>2</sup><br>17C |
| 50%        | $t_{on} = 20 \text{ ms}$             | $t_{on} = 6.66 \text{ ms}$           | $t_{on} = 2.5 \text{ ms}$            |
|            | $t_{off} = 20 \text{ ms}$            | $t_{off} = 6.66 \text{ ms}$          | $t_{off} = 2.5 \text{ ms}$           |
|            | PCD = -360 mA/cm <sup>2</sup><br>23A | PCD = -360 mA/cm <sup>2</sup><br>23B | PCD = -360 mA/cm <sup>2</sup><br>23C |
| 75%        | $t_{on} = 30 \text{ ms}$             | $t_{on} = 10 \text{ ms}$             | $t_{on} = 3.75 \text{ ms}$           |
|            | $t_{off} = 10 \text{ ms}$            | $t_{off} = 3.33 \text{ ms}$          | $t_{off} = 1.25 \text{ ms}$          |
|            | PCD = -240 mA/cm <sup>2</sup><br>32A | PCD = -240 mA/cm <sup>2</sup><br>32B | PCD = -240 mA/cm <sup>2</sup><br>32C |

test was performed in DUCOM UNITEST 250 where Rockwell C type diamond indenter was used. Corrosion analysis of the obtained Zn coating was done by a Corrtest electrochemical workstation in 3.5% NaCl solution at a scan rate of 0.1667 mV/s. Electrochemical impedance spectroscopy (EIS) spectra were acquired at room temperature in the frequency range of  $10^5$ –0.01 Hz and 10 mV at corrosion potential.

### 3 Results and Discussion

For DC deposition, the coating was obtained at all current densities for 5 min with magnetic stirring at 300 rpm.

Figure 2a shows the variation of the stylus height over the surface and coating, which has been used to determine the coating thickness and roughness. The roughness and thickness of all other DC and pulse depositions were measured and are presented in Fig. 2c, d. The thickness of the coated surface was also obtained by a cross-sectional SEM micrograph (Fig. 2b). The thickness values obtained by the surface profiler and SEM for the  $-150$  mA/cm<sup>2</sup> deposition are almost complimenting each other. It can be noticed that both the roughness and thickness values are increasing with an increase in current density during the DC deposition. This could be due to the high rate of reduction of metallic ions

which has led to fast nucleation and growth [14]. The thickness of the Zn coatings has been observed to be between 13 and 28  $\mu$ m. The average roughness and thickness of pulsed coated are higher for high PCD ( $-720$  mA/cm<sup>2</sup>) and low duty cycle (25%). It can further be observed that the average thickness is increasing at the frequency of 25 Hz with the duty cycle.

### 4 Corrosion Behavior of the As-Deposited Films

Figure 3 shows the polarization curve of Zn-coated surface deposited with different current densities and pulse parameters.

The values of corrosion potential ( $E_{\text{Corr}}$ ), corrosion current density ( $i_{\text{Corr}}$ ) and corrosion rate are obtained through Tafel extrapolation and are presented in Table 2.

The coating of current density  $-250$  mA/cm<sup>2</sup> is showing the least corrosion rate and maximum for  $-150$  mA/cm<sup>2</sup>. The corrosion behavior of the deposited surface depends on the structure of the deposits and its related nucleation process during the deposition. Accordingly, the impact of grain architecture has been explained in the succeeding sections. The corrosion behavior of the pulsed deposited coatings is presented in Table 2.

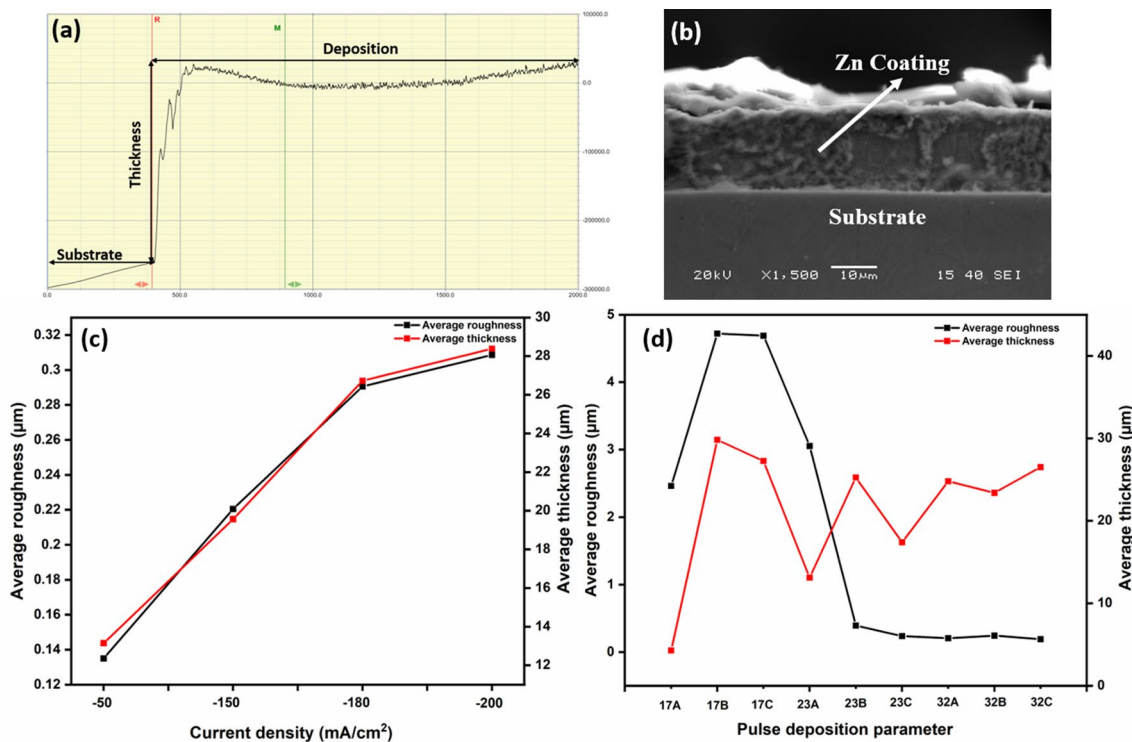


**Fig. 2** a Thickness profile of coated Zn on MS, b cross section of coated Zn at the current density of  $-150$  mA/cm<sup>2</sup>, average roughness and thickness of Zn deposition at c DC and d pulse conditions

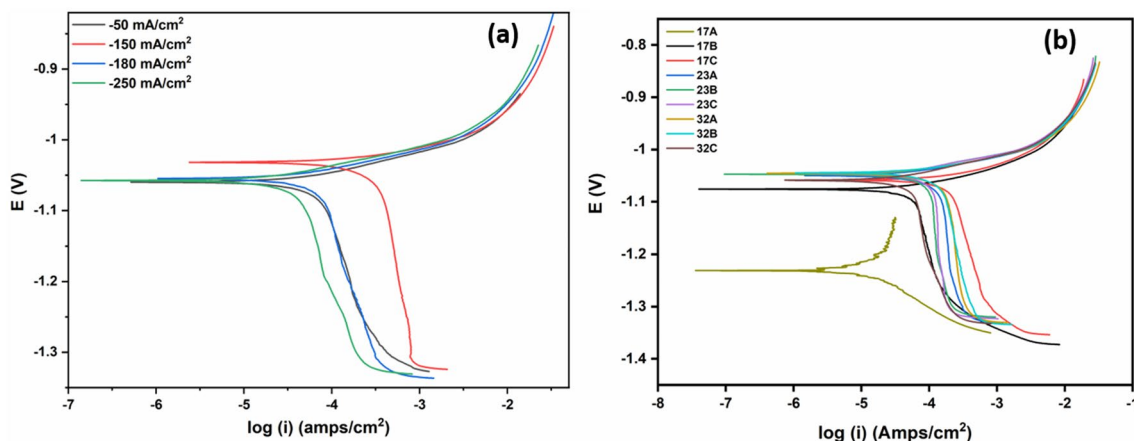


**Fig. 3** Polarization curve of deposited Zn on MS via **a** DC and **b** Pulse deposition in 3.5 wt% NaCl solution

**Table 2** Corrosion parameters obtained from Tafel fit for Zn films

| Deposition parameter | Polarization data |                |                                    |                    |                        |
|----------------------|-------------------|----------------|------------------------------------|--------------------|------------------------|
|                      | $\beta_a$ (mV)    | $\beta_c$ (mV) | $i_{Corr}$ (Amps/cm <sup>2</sup> ) | $E_{Corr}$ (Volts) | Corrosion Rate (mm/yr) |
| -50                  | 28.51             | 93.28          | $3.71 \times 10^{-5}$              | -1.05              | 0.558                  |
| -150                 | 21.71             | 62.80          | $1.17 \times 10^{-4}$              | -1.03              | 1.757                  |
| -180                 | 23.03             | 42.30          | $2.33 \times 10^{-5}$              | -1.05              | 0.350                  |
| -250                 | 26.62             | 49.31          | $1.56 \times 10^{-5}$              | -1.05              | 0.234                  |
| 17A                  | 61.09             | 42.09          | $6.78 \times 10^{-6}$              | -1.23              | 0.102                  |
| 23C                  | 20.62             | 29.67          | $2.79 \times 10^{-5}$              | -1.04              | 0.419                  |
| 32C                  | 29.90             | 75.14          | $2.64 \times 10^{-5}$              | -1.05              | 0.396                  |

From Table 2, it has been found that corrosion potential is almost equal (-1.04–-1.07 V) for all parameters of pulse-deposited coatings except for 17A. For higher PCD (-720 mA/cm<sup>2</sup>) at a higher frequency (200 Hz), the corrosion rate is high, whereas it is lesser at the frequency of 25 Hz. With the deposition synthesized at the peak current density of -360 mA/cm<sup>2</sup>, less corrosion rate is found at a higher frequency (200 Hz) and a higher corrosion rate is found at a lower frequency (25 Hz). At lower peak current density (-240 mA/cm<sup>2</sup>), the corrosion rate is lower at higher frequency (200 Hz). From Table 2, it can be seen that the corrosion resistance of the coatings is good for 17 B, 23 C and 32 C. The rest of the films are giving fair corrosion resistance except only 17 C. From Table 2, it can generally be observed that higher peak current density gives better corrosion resistance at the frequency of 25 Hz, whereas at lower peak current density it has been found that the corrosion rate is more. The corrosion resistance is better than the DC-plated films. The possible reason for the observation is presented below through a thorough investigation of the structural and composition analysis of the films before and after corrosion.

### 5 Structure, Composition and Phase Analysis in Pre and Post-Corrosion Conditions

Figure 4 depicts the SEM images of DC coatings before and after the polarization test. From Fig. 4a, c, e and g it can be observed that the surface of the deposition looks uniform and dense before corrosion for all CDs. Film at -180 mA/cm<sup>2</sup> appears to have optimum uniformity and density. Though the deposition at -250 mA/cm<sup>2</sup> seems finer, the grains are tending toward dendritic in nature. Hence, with increase in deposition CD, the deposition tends to become powdery instead of a continuous film which may be due the fact that high CD would lead a high nucleation and hence a growth rate. Due to the powdery nature, some of the zinc particles are expected to get oxidized as they will have more surface area to react with the open environment.

The surfaces after corrosion (Fig. 4b, d, f and h) are distinctly different from the pre-corrosion test films. After corrosion (in Fig. 4e), grains look porous and oxidized. As compared to Fig. 4e, corroded surfaces have fewer cracks and pores for the films deposited at -180 mA/cm<sup>2</sup> and -250 mA/cm<sup>2</sup> current density (Fig. 4g). Now concentrating

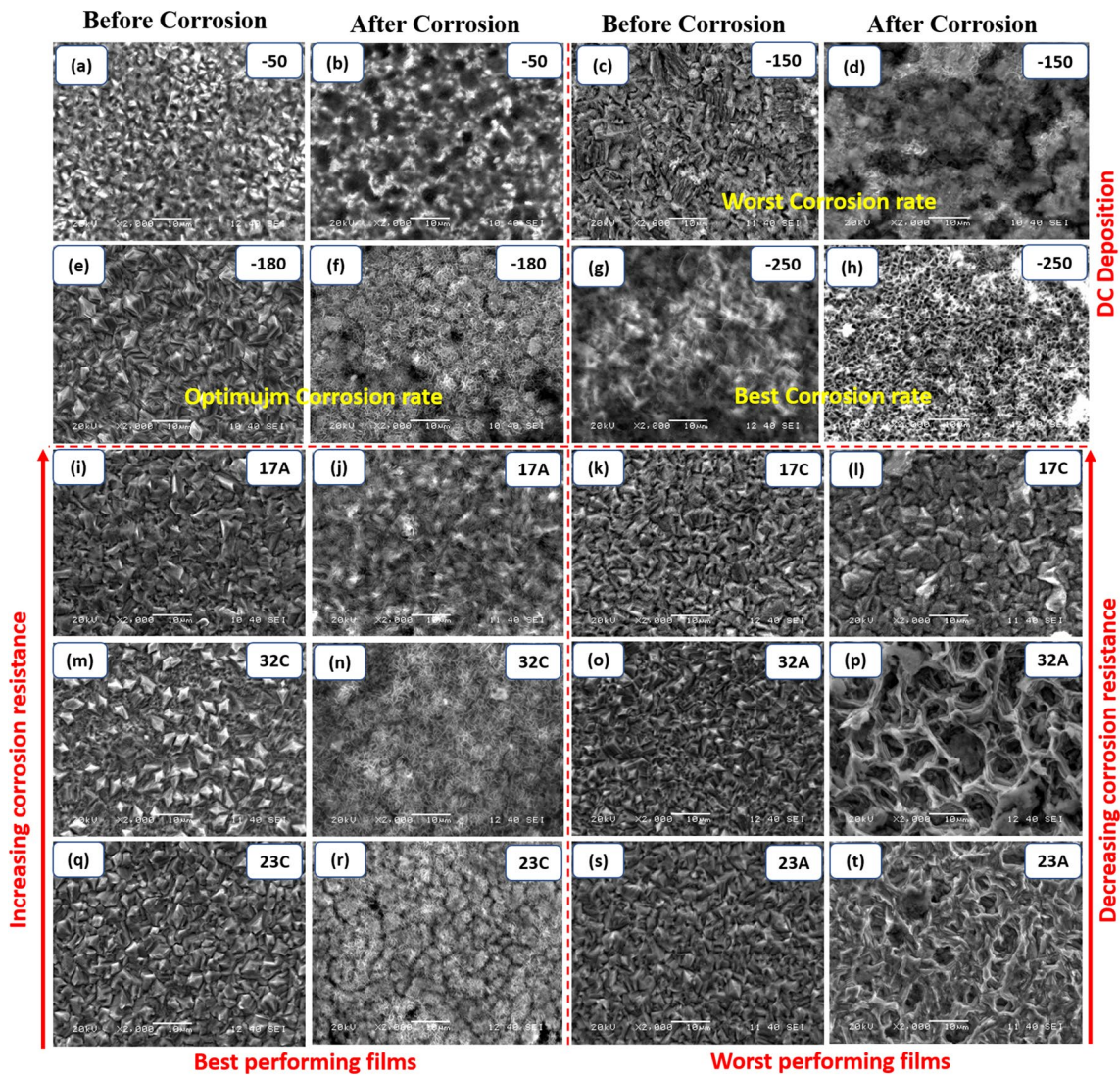


**Fig. 4** SEM of coated and corroded Zn on MS in a–h DC i–t pulsed conditions

on the films deposited at  $-180 \text{ mA/cm}^2$  and  $-250 \text{ mA/cm}^2$ , it can be seen that after corrosion it is looking more uniform and denser (Fig. 4f and h). Maximum dissolution is observed for the film of  $-50 \text{ mA/cm}^2$ . The reason for the

trend is mentioned in the subsequent sections. Figure 4i–t represents the SEM images of films coated at  $-720 \text{ mA/cm}^2$ ,  $-240 \text{ mA/cm}^2$ , and  $-360 \text{ mA/cm}^2$  peak current density for lesser corrosion rate and higher corrosion rate as

**Table 3** Parameters obtained from scratch test for DC deposition and pulse deposition

| Parameters | LC <sub>1</sub> (N) | LC <sub>2</sub> (N) | CPR   | MLHA (N) | Toughness (MPa) | Critical shear-force (MPa) | Adhesion strength (MPa) |
|------------|---------------------|---------------------|-------|----------|-----------------|----------------------------|-------------------------|
| -50        | 2.90                | 4.57                | 4.83  | 1.67     | 2750.90         | 34.25                      | 33.97                   |
| -150       | 2.53                | 4.58                | 5.19  | 2.05     | 1966.30         | 43.78                      | 36.72                   |
| -180       | 6.50                | 11.24               | 30.82 | 4.74     | 6772.42         | 93.46                      | 142.52                  |
| -250       | 2.33                | 4.35                | 4.71  | 2.02     | 2620.16         | 57.36                      | 55.56                   |
| 17A        | 4.39                | 10.79               | 28.11 | 6.41     | 5770.98         | 116.88                     | 164.75                  |
| 23C        | 6.45                | 10.13               | 23.73 | 3.68     | 4348.61         | 105.48                     | 129.33                  |
| 32C        | 5.28                | 9.45                | 22.04 | 4.18     | 6466.59         | 80.95                      | 121.30                  |

shown in Table 3. From Fig. 4i and j, one can observe that the film is dense and more uniformly deposited for condition 17A. After corrosion, the film is looking still uniform and less porous. The same variation in grain morphology of 32 C and 23 C is also observed. Figure 4m–p shows the SEM images of Zn deposition with pulse deposition at  $-240 \text{ mA/cm}^2$  peak current density and 75% duty cycle. Further, from Fig. 4m and o it can be observed that the film is dense and uniform for both parameters before corrosion, whereas after corrosion porous appearance comes up. The general observation is that, the best performing films have uniform oxide-like structures which are believed to impart good corrosion resistance. These oxide layers must have been relatively impervious to the testing solution/corrosive media. The oxide films might have been formed at the high anodic polarization region during the corrosion testing. Now focusing on the films with less corrosion resistance, there are connected bird nest-like structures leading to high porosity. Because of the porosity, the corrosive media must have infiltrated through the oxide films and led to further corrosion. The oxide formation and its properties can be cross-verified through the EIS analysis which is presented in the following section. A thorough analysis of the compositional change (if

any) in different conditions of deposition was done to check whether it might have affected the said corrosion behavior and is presented in Fig. 5.

The presence of O, S, Cl, Fe and Zn has been observed on the coated as well as corroded surfaces. The presence of Cl, S, etc., may be due to some entrapped ions which came during deposition and could not be removed during washing. The percentage of oxygen is high at  $-250 \text{ mA/cm}^2$  before corrosion. Hence, it can be argued at this juncture that a surface zinc oxide might have been formed on this deposition which has provided the best corrosion resistance for the film. From Fig. 5c, one can also notice that the percentage of Zn is high for the deposition of  $-720 \text{ mA/cm}^2$  at the frequency of 75 Hz, whereas it is high for the deposition of  $-360 \text{ mA/cm}^2$  at the frequency of 200 Hz and the deposition of  $-240 \text{ mA/cm}^2$  at the frequency of 75 Hz. A higher percentage of Zn or less impurities might have led to better corrosion resistance of the films.

Figure 6 shows X-ray diffraction measurements of as-deposited and corroded Zn deposits. XRD peaks show the presence of Fe and Zn for all CDs. As the current density is increasing, the intensity of the strongest Zn plane (1 0 1) is increasing, whereas the intensity of the iron peak (1 1

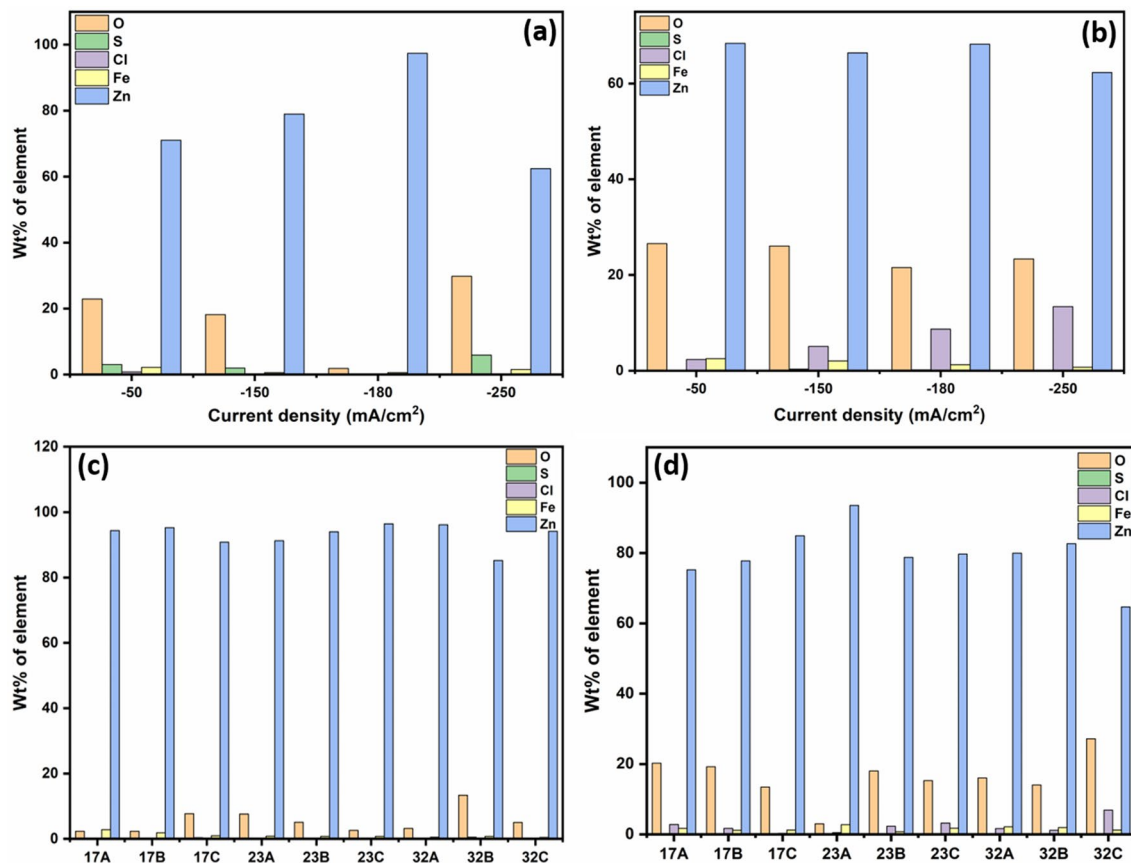
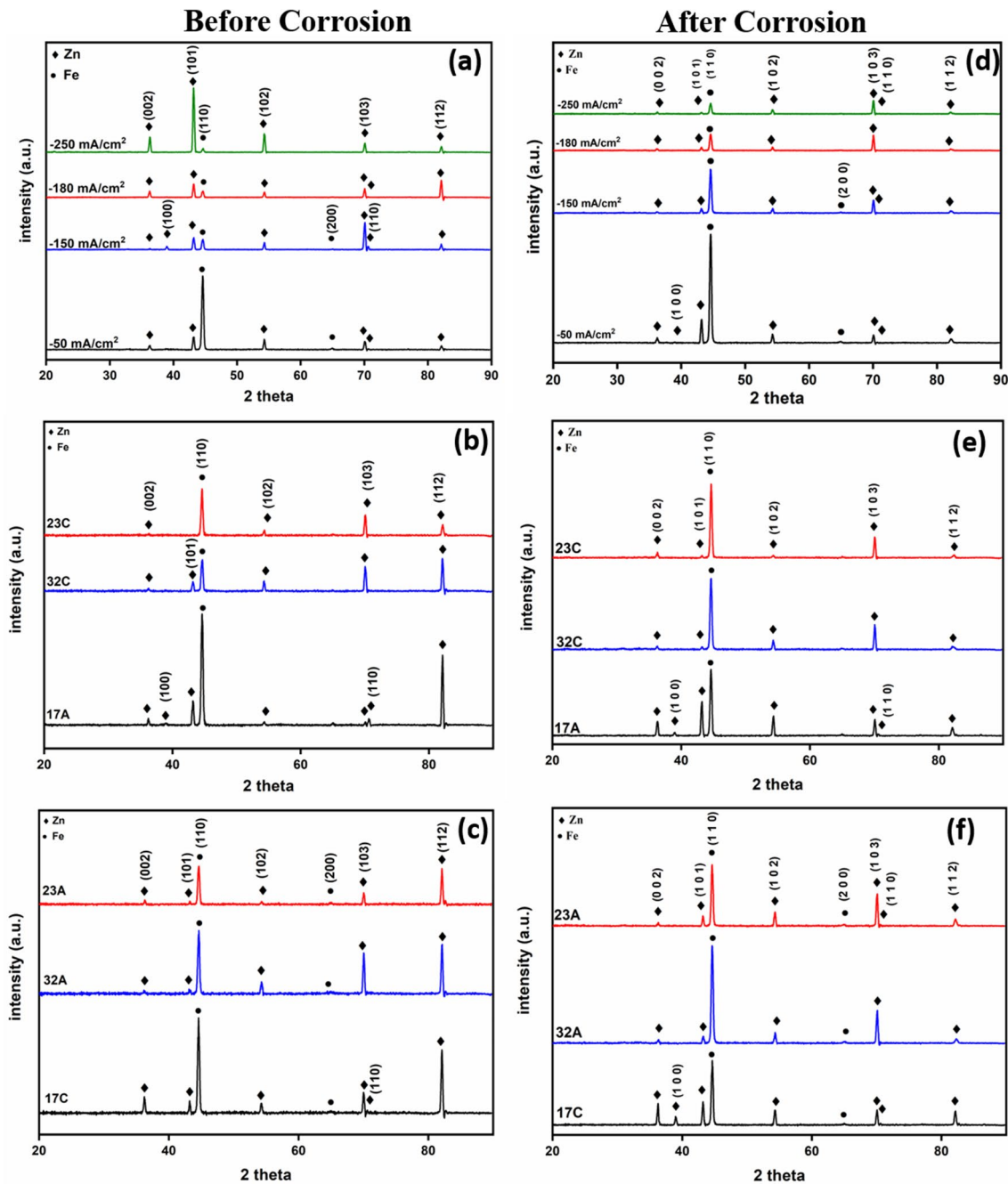


Fig. 5 Element Wt% of coated Zn on MS a as-deposited DC b corroded DC c as-deposited pulse d corroded pulse



**Fig. 6** XRD pattern of deposited Zn on MS **a, d** DC deposition, **b, e** best corrosion rate of pulse deposition, **c, f** worst corrosion rate of pulse deposition

0) is decreasing. This could be due to the thicker deposits with CD.

The intensity of Zn peaks is high for the film deposited at  $-250 \text{ mA/cm}^2$  before corrosion. Zn peak is absent for planes of (1 0 0) and (1 1 0) for the deposit of  $-250 \text{ mA/cm}^2$  current density before corrosion. From Fig. 6d it can be observed that after corrosion, iron peak is decreasing with increasing current density which shows better corrosion resistance at higher current density. Similar other observations are present in this

figure. This may indicate some crystallographic texture evolution during deposition at different current densities. This is a common phenomenon of electrodeposition and to quantify this, relative texture coefficients of different crystallographic planes of each deposit were carried out as a basic study of texture analysis. However, no significant variation has been observed, hence not been included in the present investigation. For PEPs, XRD peaks are showing the presence of iron and zinc at all deposition parameters before and after corrosion.



Figure 6b and e shows the better corrosion resistive property for all peak current densities (−720, −240, −360 mA/cm<sup>2</sup>), whereas Fig. 6c and f shows the worst corrosion resistance property for all peak current densities. After corrosion in Fig. 6e and f, it can clearly be seen that one more extra peak at the deposition of −720 mA/cm<sup>2</sup> PCD of Zn at the plane of (1 0 0) is visible and corresponds to a 2θ value of 38.99°. Figure 6c and f shows the peak of the plane (1 0 0) which is not present before corrosion for 17 C but is visible after corrosion. From Fig. 6b and e one can observe that Fe peak at the plane of (2 0 0) is absent before corrosion and after corrosion. The absence of Fe peak is showing the better quality of deposition for 17 A, 32 C and 23 C.

### 6 Adherence Analysis of Coating

From the above analysis, it can be emphasized that corrosion resistance of the electroplated zinc has been improved, and to explore the commercial use of it, adherence is one of the significant parameters. To measure the adherence, scratch testing was done through an application of load range of 1–41 N for a 4 mm stroke length. Figure 7a and b shows the nature of scratch and variation of traction force and normal load with stroke length for deposits of both conditions. LC<sub>1</sub> is the load where coating is first observed, i.e., load bearing capacity and crack initiation resistance, whereas LC<sub>2</sub> is the load where complete delamination of coating has

occurred [15]. Table 3 shows that crack initiation and complete removal of coating occurred at a higher load (6.50 N and 11.24 N) when the coating of Zn was done at −180 mA/cm<sup>2</sup> deposition current density.

From Table 3 it can be observed that the complete removal load of the coating is high for 17 A, 23 C and 32 C among all PEP parameters. These are the coatings which have good corrosion resistance also. From Eq. (1) and Eq. (2), scratch crack propagation resistance (CPR) and material load handling ability (MLHA) have been calculated to obtain the strength of the layer on the substrate [16].

$$CPR = LC_1(LC_2 - LC_1) \tag{1}$$

$$MLHA = (LC_2 - LC_1) \tag{2}$$

The CPR and MLHA for the deposits obtained at −180 mA/cm<sup>2</sup> are 30.82 and 4.74 which is the highest in the lot. CPR and MLHA are found to be varied from 22 to 29 and 3.6–6.5 N for best pulse deposition parameters as mentioned in Table 1. Toughness (H<sub>SP</sub>), critical shearing force (τ<sub>S</sub>) and adhesion strength (σ) were also calculated to obtain the ability or quality of the coating following Eqs. 3–5. Toughness is the quantity that measures the ability to sustain load without fracturing or breaking the material, which can quantify the maximum absorbing energy at which material fails. The toughness of the coating has been calculated by using Eq. 3.

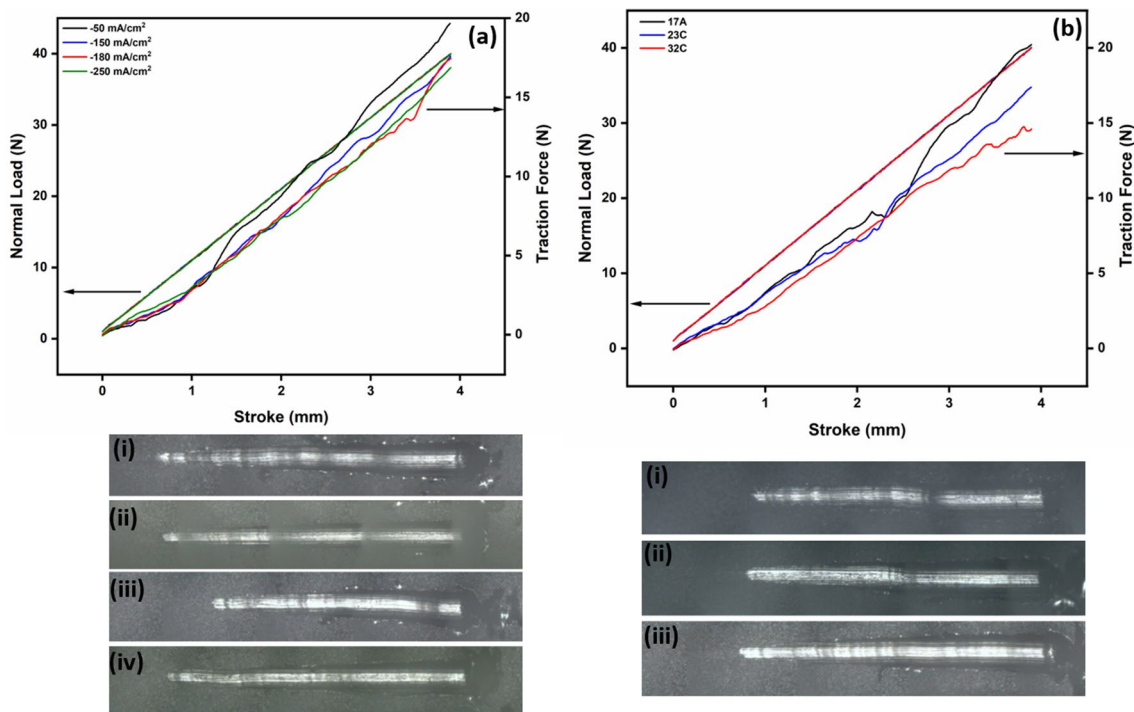


Fig. 7 Adherence curve and microscopic images of scratches of coating a DC coating, b pulse deposition

$$H_{SP} = \frac{8P}{\pi w^2} \tag{3}$$

where  $P$  = applied load at which complete coating removed ( $N$ ) and  $w$  = width of scratch (mm).

Critical shearing force ( $\tau_s$ ) is the required load to cause a material or coating to break by shear.

$$\tau_s = \frac{kAH}{(R^2 - A^2)^{0.5}} \tag{4}$$

where  $k$  = coefficient of friction,  $H$  = hardness of the substrate,  $R$  = radius of indenter (0.2 mm) and  $A$  = radius of the contact which is defined as  $A = \sqrt{\frac{LC_2}{\pi H}}$

The adhesion strength ( $\sigma$ ) of deposition may also explain the quality of coating which is also found from the parameter obtained from the scratch test. Adhesion strength measures the ability of the coating to pull off the material from the substrate. Adhesion strength ( $\sigma$ ) is obtained from Eq. (5) [17].

$$\sigma = \frac{2kLC_2}{\pi R w} \tag{5}$$

where  $R$  = radius of indenter (0.2 mm) and  $w$  = initial width of scratch where complete removal of coating is visible. From Table 3, it is obtained that the best adherence strength 142.52 MPa is obtained at the deposition of  $-180 \text{ mA/cm}^2$  current density. Pulse deposition parameter shows adherence

strengths of 164.75 MPa, 129.33 MPa and 121.30 MPa for 17A, 23 C and 32 C, respectively, which are within the best pulsed deposition regime. Hence, it can be concluded that good adherence can be an essential parameter for good corrosion resistance of the coatings.

### 7 Corrosion Mechanism Analysis by Impedance Study

From the Nyquist plot, it can clearly be seen that there are more than one semicircle loops appearing at high frequency, medium frequency and low frequency (Fig. 8). The loop at high frequency for DC-plated films is shown in the inset of Fig. 8a. The impedance curves of PEP zinc are presented in Fig. 9. The impedance at higher frequency would be for solution resistance and solid electrolyte interface formation, whereas at the lower frequency, it represents the charge exchange process at the electrical double layer [18]. The curves had been fitted with equivalent circuits (EC). The equivalent circuit diagrams are shown in Fig. 8c and d. The fitting parameters are three constant phase elements (CPE) and four resistances (R) for  $-150, -180$  and  $-250 \text{ A/cm}^2$  and pulsed-plated films. The parallel circuits of CPE and R would be for three interfaces. One more film capacitance and an inductance ( $L = 0.05$ ) at medium frequency have been found after the fit for film deposited at  $-50 \text{ mA/cm}^2$ . Accordingly, the impedance at low frequency would give

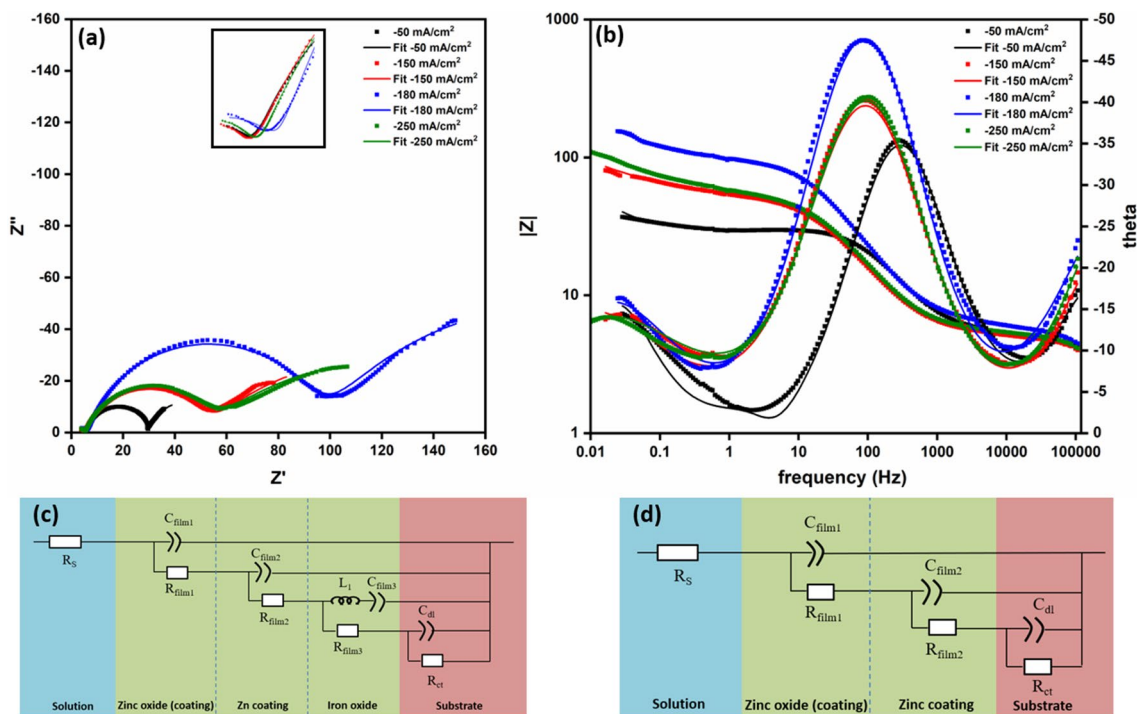


**Fig. 8** a Nyquist b Bode plot of DC-plated Zn coating during corrosion, c fitted circuit diagram for  $-50 \text{ mA/cm}^2$ , d other deposition parameter

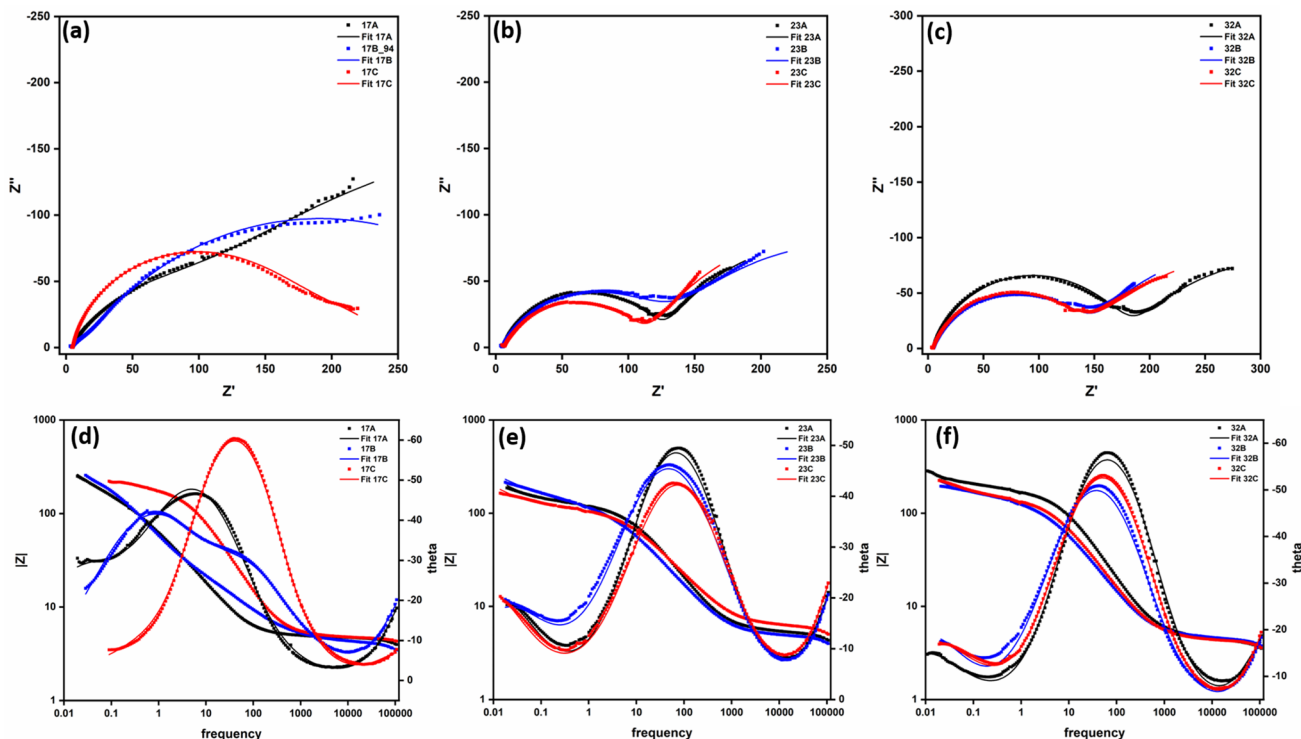


**Fig. 9** Nyquist and Bode plot of pulse-plated Zn coating during corrosion

the charge transfer resistance ( $R_{ct}$ ), whereas at the medium frequency, it could be other interface/film resistances ( $R_{film}$ ). Double-layer capacitance ( $C_{dl}$ ) and the second capacitor corresponding to the coatings ( $C_{film}$ ) have been found by Brug’s equation from the corresponding CPEs [19]. These relations are very useful to find out the mechanism. All the parameters extracted from fitting are shown in Table 4.

From the ECs, the following corrosion mechanism can be proposed. For all the DC (except  $-50 \text{ mA/cm}^2$ ) and

pulsed coatings, there are three capacitances; hence, there must be two films on the substrates. As only zinc has been coated onto MS, it is expected that the first layer exposed to corrosion solution must be the zinc oxide/hydroxide layer which might have developed during the process of corrosion. The second layer is the coated Zn. Hence, the interfaces are (i) solution and zinc oxide/hydroxide layer, (ii) zinc oxide/hydroxide layer and zinc coating and (iii) zinc coating and MS. At the onset of the corrosion process, the

**Table 4** Fitted EIS values of coated Zn on MS at different current densities

| EIS Parameter                        | Deposition current density ( $\text{mA/cm}^2$ ) |                  |                  |                | Pulse parameter |           |         |
|--------------------------------------|---|------------------|------------------|----------------|-----------------|-----------|---------|
|                                      | -50   | -150             | -180             | -250           | 17A             | 23C       | 32C     |
| $R_s$ ( $\Omega\text{-cm}^2$ )       | 2.5   | 1.78             | 1.44             | 1.28           | 1.985           | 2.01      | 1.88    |
| $CPE_{1-p}$                          | 0.89  | 0.82             | 0.73             | 0.79           | 0.98            | 1.00      | 1.00    |
| $R_{film1}$ ( $\Omega\text{-cm}^2$ ) | 2.8   | 3.39             | 4.99             | 4.15           | 2.683           | 4.04      | 2.41    |
| $CPE_{2-p}$                          | 0.80  | 0.76             | 0.81             | 0.77           | 0.72            | 0.70      | 0.78    |
| $R_{film2}$ ( $\Omega\text{-cm}^2$ ) | 24.4  | 48.1             | 91.4             | 49.6           | 132.6           | 109.50    | 139.80  |
| $CPE_{3-p}$                          | 1   | 0.54             | 0.64             | 0.51           | 0.59            | 0.69      | 0.61    |
| $R_{film3}$ ( $\Omega\text{-cm}^2$ ) | 1.98  | –                | –                | –              | –               | –         | –       |
| $CPE_{4-p}$                          | 0.88  | –                | –                | –              | –               | –         | –       |
| $R_{ct}$ ( $\Omega\text{-cm}^2$ )    | 26.27   | 118              | 171.9            | 123.3          | 543.1           | 284.90    | 322.00  |
| $C_{dl}$ ( $\mu\text{F/cm}^2$ )      | $2.3\text{E}+05$                                | $1.2\text{E}+04$ | $7.0\text{E}+03$ | $3\text{E}+03$ | 1205.65         | 19,854.75 | 3951.72 |
| $C_{f1}$ ( $\mu\text{F/cm}^2$ )      | 0.44  | 0.30             | 0.25             | 0.21           | 0.38            | 0.26      | 0.45    |
| $C_{f2}$ ( $\mu\text{F/cm}^2$ )      | 60.7  | 164.1            | 101.7            | 148.2          | 2263.68         | 166.82    | 212.05  |
| $C_{f3}$ ( $\mu\text{F/cm}^2$ )      | $7.8\text{E}+04$                                | –                | –                | –              | –               | –         | –       |

oxide layer must have been formed first which is not fully impervious. Through the porous oxide layer, the solution has passed through and reacted with the pure zinc coating. The pure zinc coating is also believed to have measurable pores as charge transfer resistance has appeared in the circuit. The analysis of film resistance would testify to the corrosion resistance tendency of the films. Starting with the solution resistance (from Table 4), it is almost invariable for all the coatings as the corroding solution is the same for all. The oxide film resistance is highest for  $-180 \text{ mA/cm}^2$ , i.e.,  $\Omega\text{-cm}^2$  and almost invariable for all other films. Also, the film resistance and charge transfer resistance are high for  $-180 \text{ mA/cm}^2$  in comparison to the deposits at  $-250 \text{ mA/cm}^2$ . One plausible explanation may be due to the fact that film at  $-180 \text{ mA/cm}^2$  has optimum uniformity and compactness with less porosity. For the EIS scan, the chosen DC potential is the corrosion potential ( $-1.05$  for both the films). During the scan, enough time is allowed to the films to get acclimatized with the solution, and due to its better compactness, a well-developed oxide/passive film has been developed on the surface of the film deposited at  $-180 \text{ mA/cm}^2$ , whereas, in case of  $-250 \text{ mA/cm}^2$ , as the deposit is powdery, the oxide film might not be continuous. Hence, the corrosion resistance of  $-180 \text{ mA/cm}^2$  is better than  $-250 \text{ mA/cm}^2$  films. Accordingly, the optimum corrosion resistance could be the one at  $-180 \text{ mA/cm}^2$  which has a combination of good corrosion resistance, less porosity (high film resistance) and good adherence to the substrate. Further film resistance ( $R_{\text{film}2}$ ) for pulse-plated Zn which comes after the oxide film is found to vary between  $109 \Omega\text{-cm}^2$  and  $178 \Omega\text{-cm}^2$  for all peak current densities except only for  $-720 \Omega\text{-cm}^2$  at the frequency of 75 Hz. From Tables 2 and 4, one can observe that charge transfer resistance is high at higher peak current density ( $-720 \text{ mA/cm}^2$ ) and lower frequency (25 Hz) which is validated from Table 2 with lower corrosion rate. For deposits at  $-50 \text{ mA/cm}^2$ , the deposit is dissolving unlike other deposits; hence, the double-layer capacitance is high and charge transfer resistance is low. Because of the dissolution of the film, the solution penetration is high and hence an oxide layer of iron might have formed on the surface, leading to the fourth capacitance on the surface. Hence, the film is not having good corrosion properties for the deposition at  $-50 \text{ mA/cm}^2$  current density.

## 8 Conclusion

In the current investigation, Zn has been electrodeposited onto MS in DC and PEP mode and the corrosion behavior was compared and analyzed. The thickness of the Zn deposit has been found to be less than  $30 \mu\text{m}$  for all the conditions. Corrosion analysis of deposited Zn was done by the Tafel

polarization technique as well as EIS. Following are the salient observations:

- Thickness and grain uniformity have been found to be increased with increase in current density and peak current density for DC and pulsed deposition respectively. Best anti-corrosive performing films are deposited at  $-250 \text{ mA/cm}^2$  current density for DC plating with a corrosion rate of  $0.234 \text{ mm/yr}$ . XRD peaks are showing the presence of Fe and Zn at all deposition parameter. It is showing that iron peak is decreasing with increasing current density. SEM images show the morphology of the coating before and after corrosion for DC deposition and pulse deposition. Before corrosion SEM images are showing dense and compact structure, whereas after corrosion it is showing oxide formation. However, from EIS analysis, the corrosion restriction tendency has been found to be best for the deposits at  $-180 \text{ mA/cm}^2$  with a corrosion rate of  $0.354 \text{ mm/yr}$ . Hence, this current density has been chosen for pulse deposition. For pulse plating, the best performing films are for parameters 17A, 23 C and 32 C with corrosion rates of  $0.102$ ,  $0.419$  and  $0.396 \text{ mm/yr}$ , respectively.
- The compositional and grain architecture analysis presents an observation that a current density of  $-180 \text{ mA/cm}^2$  has led to relatively less porous films and well-covered oxide layers (as observed from EIS analysis) which could be the main reason for such good corrosion resistance.
- Further, the adherence analysis for DC deposition also shows the best load-carrying capacity for  $-180 \text{ mA/cm}^2$  current density which validates good quality of coating in terms of adherence and corrosion resistance. Accordingly, the adherence of the films deposited at conditions of 17 A, 23 C and 32 C has good adherence as well. Finally, it can be inferred that the corrosion performance could be improved by the pulse plating method.

**Acknowledgements** The authors are thankful to Department of Metallurgical and Materials Engineering, National Institute of Technology Rourkela and Tata Steel Limited Jamshedpur for providing the equipment and financial facility.

**Author contributions** PU contributed to conceptualization, methodology, analysis, writing and draft preparation; AN provided methodology; AB contributed to conceptualization; AB performed data curation, formal analysis, and review and editing; SD performed data curation and formal analysis; AM contributed to supervision, funding acquisition, conceptualization, data curation, formal analysis, and writing—review and editing.

**Funding** The funding was supported by Tata Steel (Grant No: 3000132079/132).

## Declarations

**Conflict of interest** The authors claim that they have no apparent financial conflicts of interest or close personal connections that could have appeared to have an influence on the research described in this work.

## References

1. Karthick S, Muralidharan S, and Saraswathy V, *Arab J Chem* **13** (2020) 3301. <https://doi.org/10.1016/j.arabjc.2018.11.005>
2. Shibli S M A, Meena B N, and Remya R, *Surf Coat Technol* **262** (2015) 210. <https://doi.org/10.1016/j.surfcoat.2014.12.054>
3. Asgari H, Toroghinejad M R, and Golozar M A, *Curr Appl Phys* **9** (2009) 59. <https://doi.org/10.1016/j.cap.2007.10.090>
4. Verma A R B, and Van Ooij W J, *Surf Coat Technol* **89** (1997) 132. [https://doi.org/10.1016/S0257-8972\(96\)02941-6](https://doi.org/10.1016/S0257-8972(96)02941-6)
5. Vasilakopoulos D, Bouroushian M, and Spyrellis N, *Electrochim Acta* **54** (2009) 2509. <https://doi.org/10.1016/j.electacta.2008.11.059>
6. Bengoa L N, Bruno S, Lazzarino H A, Seré P R, and Egli W A, *Mater Sci* **8** (2015) 1174. <https://doi.org/10.1016/j.mspro.2015.04.183>
7. Dattilo M, Cole E R, and O'Keefe T J, *Conserv Recycl* **9** (1986) 55. [https://doi.org/10.1016/0361-3658\(86\)90134-7](https://doi.org/10.1016/0361-3658(86)90134-7)
8. Feng Z, Li Q, Zhang J, Yang P, and An M, *Surf Coat Technol* **270** (2015) 47. <https://doi.org/10.1016/j.surfcoat.2015.03.020>
9. Jyothender K S, and Srivastava C, *Metall Mater Trans A Phys Metall Mater Sci* **52** (2021) 364. <https://doi.org/10.1007/s11661-020-06070-y>
10. Rekha M Y, and Srivastava C, *Corros Sci* **152** (2019) 234. <https://doi.org/10.1016/j.corsci.2019.03.015>
11. Sahayata B, Kumar S, Upadhyay P, Mendon R R, and Mallik A, *Mater Lett* **351** (2023) 135013. <https://doi.org/10.1016/j.matlet.2023.135013>
12. Fathy N, Kobayashi R, and Ichimura M, *Mater Sci Eng B Solid-State Mater Adv Technol* **107** (2004) 271. <https://doi.org/10.1016/j.mseb.2003.11.021>
13. Ataie S A, and Zakeri A, *Surf Coat Technol* **359** (2019) 206. <https://doi.org/10.1016/j.surfcoat.2018.12.063>
14. Doğan F, Uysal M, Duru E, Akbulut H, and Aslan S, *J Asian Ceram Soc* **8** (2020) 1271. <https://doi.org/10.1080/21870764.2020.1840704>
15. Ollendorf H, and Schneider D, *Surf Coat Technol* **113** (1999) 86. [https://doi.org/10.1016/S0257-8972\(98\)00827-5](https://doi.org/10.1016/S0257-8972(98)00827-5)
16. Kabir M S, Munroe P, Zhou Z, and Xie Z, *Wear* **380–381** (2017) 163. <https://doi.org/10.1016/j.wear.2017.03.020>
17. Sahu R K, Mukherjee D, Tiwari J P, Mishra T, and Pathak L C, *J Mater Chem* **19** (2009) 6810. <https://doi.org/10.1039/b908080e>
18. Ju H, Wu J, and Xu Y, *J Chem Sci* **125** (2013) 687. <https://doi.org/10.1007/s12039-013-0407-9>
19. Ayagou M D D, Tran T T M, Tribollet B, Kittel J, and Duret-Thual C, *Electrochim Acta* **282** (2018) 775. <https://doi.org/10.1016/j.electacta.2018.06.052>

**Publisher's Note** Springer Nature remains neutral with regard to jurisdictional claims in published maps and institutional affiliations.

Springer Nature or its licensor (e.g. a society or other partner) holds exclusive rights to this article under a publishing agreement with the author(s) or other rightsholder(s); author self-archiving of the accepted manuscript version of this article is solely governed by the terms of such publishing agreement and applicable law.